

# Effect of the Protonation Degree of a Self-Assembled Monolayer on the Immobilization Dynamics of a [NiFe] Hydrogenase

Tillmann Utesch,<sup>†</sup> Diego Millo,<sup>†,‡</sup> Maria Ana Castro,<sup>§</sup> Peter Hildebrandt,<sup>†</sup> Ingo Zebger,<sup>†</sup> and Maria Andrea Mroginski<sup>\*,†</sup>

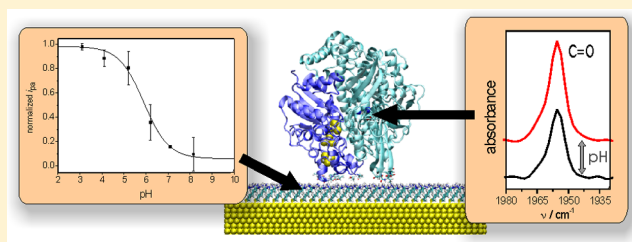
<sup>†</sup>Institut für Chemie, Technische Universität Berlin, Sekretariat PC 14, 10623 Berlin, Germany

<sup>‡</sup>Biomolecular Spectroscopy/LaserLaB Amsterdam, Vrije Universiteit Amsterdam, De Boelelaan 1083, NL-1081 HV Amsterdam, The Netherlands

<sup>§</sup>Departamento de Química Inorgánica, Analítica y Química Física/INQUIMAE-CONICET, Facultad de Ciencias Exactas y Naturales, Universidad de Buenos Aires, Ciudad Universitaria, Pabellón 2, Piso 1, C1428EHA Buenos Aires, Argentina

## Supporting Information

**ABSTRACT:** Understanding the interaction and immobilization of [NiFe] hydrogenases on functionalized surfaces is important in the field of biotechnology and, in particular, for the development of biofuel cells. In this study, we investigated the adsorption behavior of the standard [NiFe] hydrogenase of *Desulfovibrio gigas* on amino-terminated alkanethiol self-assembled monolayers (SAMs) with different levels of protonation. Classical all-atom molecular dynamics (MD) simulations revealed a strong correlation between the adsorption behavior and the level of ionization of the chemically modified electrode surface. While the hydrogenase undergoes a weak but stable initial adsorption process on SAMs with a low degree of protonation, a stronger immobilization is observable on highly ionized SAMs, affecting protein reorientation and conformation. These results were validated by complementary surface-enhanced infrared absorption (SEIRA) measurements on the comparable [NiFe] standard hydrogenases from *Desulfovibrio vulgaris* Miyazaki F and allowed in this way for a detailed insight into the adsorption mechanism at the atomic level.



## INTRODUCTION

Adsorption and immobilization of biomolecules on support materials play an important role in a wide field of research. *Inter alia*, catalysis involving immobilized enzymes on conductive surfaces is of particular interest in biotechnology and sustainable energy production. With respect to biofuel production, hydrogenases are interesting candidates, because of their ability to reversibly cleave hydrogen in several aerobic (and anaerobic) microorganisms.<sup>1–3</sup> In particular, a biological activity in the presence of oxygen will offer promising applications for clean technological fuel production with hydrogen as an energy carrier.<sup>2,4,5</sup> Hydrogenases are classified by their metal composition of the active site as [NiFe], [FeFe], and [Fe] hydrogenases.<sup>6,7</sup> The [NiFe] hydrogenase of *Desulfovibrio gigas* is a heterodimer consisting of a small and a large subunit, which are not covalently bound to each other.<sup>8</sup> It belongs to the standard or oxygen-sensitive hydrogenases, where small amounts of oxygen inhibit their catalytic activity.<sup>9</sup> At the active center of [NiFe] hydrogenases, four cysteine residues coordinate the Ni atom, two of them bridge the Ni and the Fe. In addition to these two bridging cysteines, the Fe atom is bound to one CO and to two CN<sup>-</sup> ligands, which have been validated by infrared spectroscopy.<sup>10</sup> The open-coordination position is occupied by a small ligand, such as OH<sup>-</sup>, H<sup>-</sup>, or presumably OOH<sup>-</sup>, characteristic of the different redox states

of the hydrogenase.<sup>11</sup> Details of the catalytic cycle and the bridging ligands are still under discussion.<sup>12,13</sup>

For the development of biofuel cells, the interaction of the [NiFe] hydrogenase with bare or chemically modified electrode surfaces is a crucial point.<sup>2</sup> First successful applications have been achieved but with small turnover rates and limited stability over time.<sup>4,14</sup> Therefore, studies dedicated to the optimization of such systems are required.<sup>15,16</sup>

Because structural information on the atomic level is difficult to obtain experimentally, molecular dynamics (MD) simulations are an approved and well established technique to investigate the initial adsorption processes of biomolecules on surfaces.<sup>17–23</sup> This theoretical technique may be in many cases computationally demanding, because all protein and surface atoms and often the solvent molecules are taken explicitly into account. In addition, dependent upon the size of the protein and surface properties, the length of these simulations may even go beyond several hundreds of nanoseconds. For example, it has been shown by Wei et al.<sup>22</sup> that lysozyme requires at least 70 ns to adsorb on polyethylene surfaces. In a similar way, Zuo et al.<sup>23</sup> demonstrated that 500 ns simulations are necessary for

Received: September 10, 2012

Revised: November 1, 2012

Published: December 7, 2012

properly predicting the adsorption properties of a villin headpiece onto graphene.

In this work, we applied MD simulations on a standard [NiFe] hydrogenase, serving as a relative simple and well-studied test system, which is placed on a gold electrode chemically modified with a self-assembled monolayer (SAM), to investigate the influence of the electric field strength resulting from different degrees of SAM terminal functional group ionization. Higher levels of protonation leading to a stronger electric field are expected to enhance the adsorption of the [NiFe] hydrogenase. This, however, might be on costs of the protein stability, as reported for cytochrome *c*.<sup>21</sup> Goals of this study combining experimental and theoretical techniques are, *inter alia*, to identify important binding patterns and the optimal surface configuration at an initial stage of the protein adsorption process that allow for a stable biomolecule immobilization on the monolayer system.

## MATERIALS AND METHODS

**Experimental Work. SAM Titration.** The  $pK_a$  value of the amino-terminated SAM was determined by cyclic voltammetry (CV), according to the procedure described by Degefa et al.<sup>24</sup> Briefly, the SAM-coated Au electrode exposed to a 10 mM buffered solution at the pH of interest was incubated for 10 min with a 10  $\mu$ M solution of the electroactive compound  $K_3Fe(CN)_6$ . Afterward, the  $K_3Fe(CN)_6$  solution was replaced with the corresponding buffer solution at the same pH, so that the electroactive compound was only present in the adsorbed state. The amount of the negatively charged  $[Fe(CN)_6]^{3-}$  complex adsorbed on the SAM is dependent upon the protonation state of the SAM itself and was determined by CV measurement. Given the electrochemical reversibility of the surface-confined  $[Fe(CN)_6]^{3-}$  anions (see Figure S1A of the Supporting Information), the normalized peak currents of the baseline-corrected CV traces (see Figure S1B of the Supporting Information) are plotted versus the pH (Figure 1) to yield the titration curve of the SAM.

**Surface-Enhanced Infrared Absorption (SEIRA) Measurements.** SEIRA experiments were carried out in a Kretschmann attenuated total reflection (ATR) configuration using a silicon crystal coated with a nanostructured gold film, formed by electrodeless deposition. This surface was covered with a SAM formed by immersing the Au electrode for 18 h in a 1 mM solution of 6-amino-1-hexanethiol

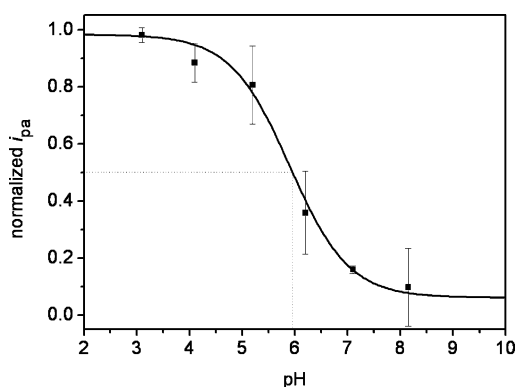


**Figure 1.** Normalized peak intensities  $i_{pa}$  (■), as derived from the CV traces obtained for the  $K_3Fe(CN)_6$  adsorbed onto the SAM-coated Au electrode at different pH values (see Figure S1 of the Supporting Information). The line represents the fit to the experimental data points. An estimate of the degree of SAM protonation at different pH values has been inferred from the fit of the normalized  $i_{pa}$  versus pH plot, assuming that  $i_{pa}$  is proportional to the amount of protonated terminal functional groups of the SAM. These percentages are  $52 \pm 9$ ,  $30 \pm 9$ , and  $16 \pm 5\%$  for pH 6.0, 6.5, and 7.0, respectively.

containing 80% ethanol and 20% water (volume percent). Subsequently, the coated electrode was rinsed with ethanol and gently dried with Ar. The protein was immobilized by covering the electrode with a 1  $\mu$ M solution of *Desulfovibrio vulgaris* Miyazaki F (*DvMF*) dissolved in 10 mM phosphate buffer at pH values of 6.0 and 7.0. After a 45 min immobilization (i.e., when 90% of the adsorption process is completed),<sup>15</sup> the protein solution was exchanged by a 10 mM phosphate buffer at pH 6.0. To determine the nature of the interaction between the protein and the surface, the intensity of the amide bands was followed spectroscopically for 3.5 h, and afterward, increasing concentrations of KCl (0.1, 0.5, 1, 1.5, 2, and 3 M) were successively added. Finally, the solution was exchanged for a 10 mM phosphate buffer at pH 6.0 for a better comparison to the initial conditions.

**Theoretical Studies. Protein.** The theoretical adsorption study was performed with the [NiFe] hydrogenase of *Desulfovibrio gigas*.<sup>8</sup> This species shows a high similarity, more than 67%, to the homologous [NiFe] hydrogenase in *DvMF* and has already been proven to predict adequately the behavior of the *DvMF* on biocompatible surfaces.<sup>15</sup> The active site was modeled in the  $Ni_4-S$  state. In this configuration, the bridging position between Fe and Ni of the active site is unoccupied. The initial conformation of one heterodimeric standard [NiFe] hydrogenase containing the small subunit that accommodates three iron sulfur (FeS) clusters and the large subunit harboring the active site was extracted from the X-ray structure (2FRV)<sup>8</sup> (Figure 2A). Despite the relatively low resolution

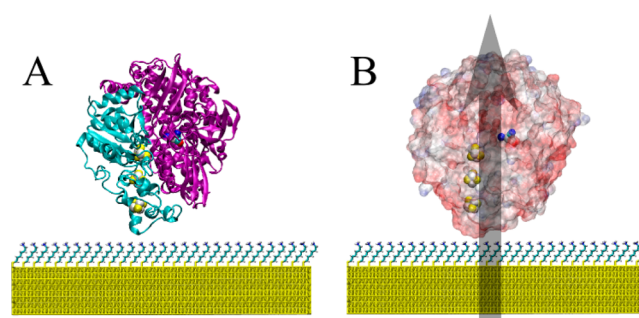


**Figure 2.** Initial positioning of the [NiFe] hydrogenase on the SAM-coated gold surface. Panel A shows the hydrogenase backbone and secondary structure elements indicating the large and small subunits in violet and cyan, respectively. Panel B shows the electrostatic potential surface of the enzyme in the same orientation with respect to the surface as in panel A. Negatively charged regions are colored in red, and positively charged areas are colored in blue. The shaded gray arrow in panel B indicates the dipole moment of the enzyme. FeS clusters and the active site are displayed as spheres in both illustrations.

(2.54 Å) of this structure compared to other anaerobic hydrogenases, we selected this topology, because it exhibits the inorganic ligand configuration at the active site that has been validated by spectroscopy<sup>10</sup> and theory.<sup>25</sup>

For the MD simulations, the titrable amino acid site chains were protonated according to pH 7.0 with the CHARMM package<sup>26</sup> and PROPKA.<sup>27</sup> This last one did not predict strong  $pK_a$  changes adjacent to the SAM. According to PROPKA, the highest stability of the [NiFe] hydrogenase is predicted to be at pH 7.2.<sup>28</sup> Histidine residues were protonated on their  $N_\delta$  (HSD state) unless the environment suggests another configuration, such as the double-protonated histidines (H193 of the small subunit and H525 of the large subunit) and the  $N_\epsilon$ -protonated residues (H45 and H185 of the small subunit and H20, H106, H114, H179, H322, H335, and H349 of the large subunit). Glutamic acids (Glu) and aspartic acids (Asp) were taken to be deprotonated, while lysine (Lys) and arginine (Arg) residues were protonated. The C-terminal residues Ala-264 of the small subunit and His-536 of the large subunit were modeled as deprotonated, and the N-termini as protonated. Given the high stability of the protonation state of most residues to variations of the pH value, all MD simulations were performed using the same protonation configuration. In total,

this protonation setting results in a total charge of  $-10 e^-$  for the enzyme, including its cofactors, which reasonably agrees with the PROPKA prediction,<sup>28</sup> and a strong dipole moment of  $\sim 1050$  D. The predicted electrostatic properties lead to the assumption of a strong Coulombic interaction with charged devices and a favorable orientation following the overall dipole moment of the hydrogenase.<sup>15,16</sup>

For electrostatic interactions, we applied the partial charges derived by Teixeira et al.,<sup>29</sup> while the van der Waals parameters were transferred from the universal force field.<sup>30</sup> Because of the lack of bonding parameters in the CHARMM27 force field, we treated the active site and the iron sulfur clusters as rigid bodies with strongly restricted internal motions during all calculations.

**Surface.** The model surface used for the simulations consists of a ca.  $121 \times 120 \text{ \AA}^2$  large Au(111) slab coated with a SAM. The sulfur atoms of the alkanethiol monolayer were placed in a  $\sqrt{3} \times \sqrt{3}$  lattice on the Au(111), resulting in a herringbone structure with a minimal separation of  $4.98 \text{ \AA}$  between two sulfur atoms.<sup>31</sup> All SAM backbones were initially tilted by ca.  $30^\circ$  to the surface normal. In total, the Au(111) was covered by 672 monolayer chains, which were chemisorbed via their sulfur atoms to the gold surface. Each chain of the SAM was composed of six carbon backbone atoms and terminated by an amino group (see Figure S2 of the Supporting Information). The level of ionization of the SAM was set to 0, 8, 33, and 50%, which resulted in a total charge of +0, +56, +224, and +336  $e^-$  for the SAM, respectively. For clarity, the corresponding models were named sim0, sim8, sim33, and sim50 according to the protonation level of the SAM. The SAM amino groups were protonated in a systematic and homogeneous way, avoiding islands of charged or uncharged SAMs. The levels of ionization chosen for the theoretical models were approximated according to the experimentally determined  $pK_a$  values at pH 6.0, 6.5, and 7.0 (52, 30, and 16% ionization levels, respectively). To avoid systems of different ionic strength resulting from the charge neutralization of the SAMs with unequal protonation levels, the bottom layer of the gold slab was slightly charged to neutralize the SAM charge of all systems. In doing so, the  $z$  dimension of the cell had to be increased by  $50 \text{ \AA}$  to avoid artificial interactions of the hydrogenase with the surface of the image cell.

To maintain the coverage pattern during the MD simulations, the gold and sulfur atoms of the SAMs were kept fixed to their positions. Thus, only non-bonding parameters derived by Bizzarri et al.<sup>32</sup> were required for the gold atoms. The monolayer was handled with the CHARMM force field for lipids, as reported earlier.<sup>19,33</sup>

**Simulation.** The initial protein–surface configurations were constructed by placing the enzyme in a minimal separation distance of  $5 \text{ \AA}$  with respect to the corresponding surface, defined as the closest contact between enzyme and SAM. In addition, the protein is initially oriented with its dipole moment normal to the gold layer (Figure 2B). The choice of this initial configuration is supported by the energy landscapes shown in Figure 3 for the sim33 model and in Figure S3 of the Supporting Information for the remaining models. These plots were obtained by computing the *in vacuo* interaction energy between the SAM surface and the protein in different orientations. Each conformation was constructed by stepwise rotating the enzyme around the  $x$  axis ( $\Phi$  angle) and the  $y$  axis ( $\Psi$  angle), maintaining the separation distance to the SAM at  $5 \text{ \AA}$ . As expected, the two most favorable energy regions correspond to conformations of the hydrogenase, where its dipole moment lies normal to the surface. In this orientation, the small subunit is facing the monolayer with its distal iron sulfur cluster and its negatively charged patch containing several glutamate residues, namely, Glu-195, Glu-198, Glu-207, and Glu-216.<sup>15,16</sup>

For the all-atom MD simulations, the NAMD 2.7 code<sup>34</sup> with the CHARMM32 force field<sup>35</sup> was used. The protein–surface system was solvated in a  $120 \times 120 \times 235 \text{ \AA}^3$  large TIP3P water box,<sup>36</sup> which was added with VMD 1.8.7.<sup>37</sup> The ionic strength mimicked by  $\text{Na}^+\text{Cl}^-$  was set to 18 mM, as used in experiments. The resulting models included more than 310 000 atoms.

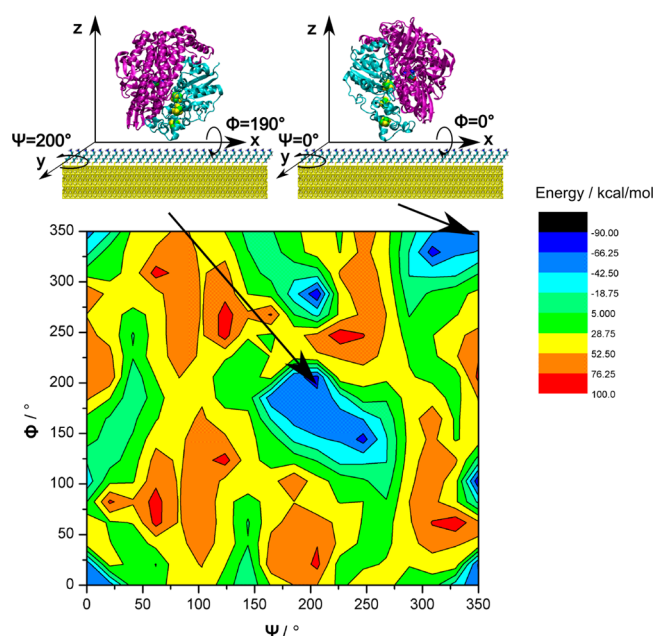


**Figure 3.** Interaction energy between hydrogenase and the SAM surface in model sim33 for different orientations of the enzyme obtained by stepwise rotating it around the  $x$  and  $y$  axes ( $\Phi$  and  $\Psi$  angles). Negative energy wells, in blue, show favorable conformations of the hydrogenase on the surface. The two most favorable geometries in interaction energy are depicted above. These two regions correspond to the same orientation of the enzyme on the surface but rotated by  $180^\circ$  along the surface normal. In both conformations, the dipole moment of the enzyme is normal to the surface.

All simulations were carried out under periodic boundary conditions with a time step of 2 fs, and all bonds to hydrogen atoms were kept fixed by the SHAKE algorithm.<sup>38</sup> For van der Waals interactions and real space electrostatics, a simple cutoff of  $12 \text{ \AA}$  was applied, while long-range electrostatics were calculated with the particle mesh Ewald summation.<sup>39</sup> Recently, the stability of this method has been evaluated and validated for systems containing charged particles.<sup>40</sup>

At first, the energy of the systems was minimized by applying the conjugated gradient algorithm for 30 000 steps until a constant total energy was achieved. During this step, the initial position constraints of  $25 \text{ kcal mol}^{-1} \text{ \AA}^{-2}$  on all heavy atoms, except the fixed gold film and SAM sulfur atoms, were decreased stepwise to  $5 \text{ kcal mol}^{-1} \text{ \AA}^{-2}$ . Then, the systems were heated for 20 ps to 300 K by constraining the motions of the heavy atoms of the protein and SAM by a force of  $5 \text{ kcal mol}^{-1} \text{ \AA}^{-2}$ . Afterward, the water and the cell size in the  $z$  direction were carefully equilibrated for 60 ps by further decreasing the position constraints to  $2.5 \text{ kcal mol}^{-1} \text{ \AA}^{-2}$ . This step is important to obtain thermal ambient temperature properties, because the following 20 ns long MD simulations were performed in a NVT ensemble. During this production run, the protein was allowed to move freely but the SAM backbone in systems with charged monolayers was lightly constrained by  $2.5 \text{ kcal mol}^{-1} \text{ \AA}^{-2}$  to maintain the coverage pattern. As stated recently, these restrictions on the monolayer should not strongly influence the adsorption behavior of enzymes<sup>41</sup> and were necessary to avoid SAM defects caused by the attraction between SAM head groups and the charged gold, especially under high SAM protonation. Simulations of the hydrogenase in the absence of the surface, the so-called bulk model, were performed using the same protocol as previously described. The total energy of each model is plotted as a function of time in Figure S4 of the Supporting Information. For all models, with the exception of model sim50, the steady curves reflect equilibrated systems that can be used for investigating the very early steps of the adsorption dynamics.

In all production runs, various protein properties, such as the root-mean-square deviation (rmsd) and root-mean-square fluctuation

(rmsf), dipole moment, and radius of gyration, as well as interaction forces, energies, number of contacts, and separation distances to the surface were evaluated in intervals of 25 ps.

## RESULTS AND DISCUSSION

**Experiments. SAM Titration.** The titration curve of the amino-terminated SAM over the whole pH value scale provides the relationship between the experimentally applied pH value and the corresponding level of SAM protonation (Figure 1). This information is required for generating an appropriate theoretical model, where a fixed protonation configuration is adopted during the calculation.

The course of the titration curve (Figure 1) displays a nearly constant value for the level of ionization above pH 7.0 and reveals a  $pK_a$  value of about  $6.0 \pm 0.2$  for the amino-terminated SAM. In contrast to this observation, the change in protonation around pH 6.0 is sensitive to very small pH variations, as reflected by the steep slope in this region. While at pH 7.0, the percentage of SAM protonation is  $16 \pm 5\%$ , and it is strongly increased at pH 6.0, reaching a value of  $52 \pm 9\%$ .

**SEIRA Adsorption Study.** In the context of our studies, the SEIRA spectroscopic measurements offer details about three important points. They afford information about (a) the protein adsorption and changes in the competitive binding with buffer ions, (b) the possible reorientation as well as possible structural reorganization at different binding conditions, and (c) the type of binding interaction with the SAM.

Figure 4 displays the IR intensities of the amide I band, which is characteristic of the protein backbone, as a function of

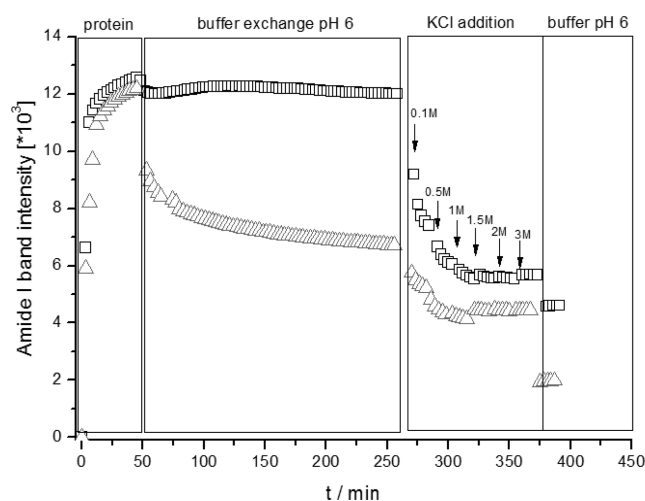


**Figure 4.** Intensity of the amide I band of the (*DvMF* [NiFe]) hydrogenase derived from SEIRA spectra. The first period of 45 min displays the immobilization of the enzyme at two different pH values of 6.0 ( $\Delta$ ) and 7.0 ( $\square$ ). In a second step, the effect of a buffer replacement at pH 6.0 is demonstrated. Afterward, KCl is added stepwise before the buffer is again exchanged with fresh solution at pH 6.0.

time, pH value, and ionic strength of the buffer solution. For the initial immobilization period of 45 min, a similar time course of the protein adsorption can be observed at pH 6.0 and 7.0. However, the amount of residual immobilized hydrogenase differs significantly after replacing the protein solution by pure buffer at pH 6.0 for the two different incubation pH conditions. The hydrogenase immobilized at pH 7.0 remains on the SAM, while the ratio between the amide I and amide II bands

decreases slightly after the replacement of the buffer solution (see Figure S5 of the Supporting Information), suggesting minor protein reorientation (*vide infra*).

In contrast to the stable adsorption at pH 7, a significant fraction of the enzyme immobilized at pH 6.0 desorbs after exchanging the buffer (Figure 4). This observation might be related to an increased buffer adsorption on the SAM under these conditions (Figure 5). While only small amounts of the

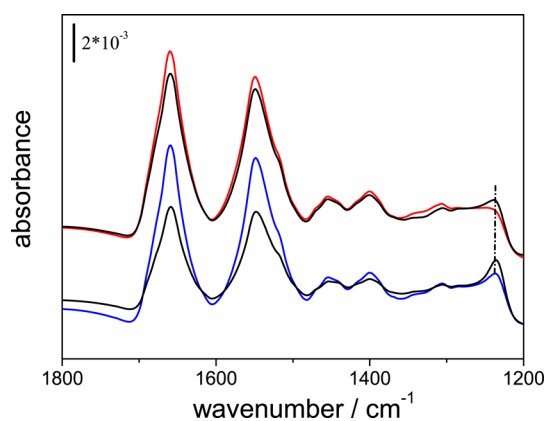


**Figure 5.** SEIRA spectra of the immobilized hydrogenase after replacement of the solution to a buffer at pH 6 (black), for an initial solution at pH 7 (red) and pH 6 (blue), respectively. Of particular interest are the amide I and amide II absorptions at  $1660$  and  $1549$   $\text{cm}^{-1}$  as well as the band at  $1240$   $\text{cm}^{-1}$ , assigned tentatively to a  $\nu_s(\text{P}=\text{O})$  vibration of the phosphate buffer.

negatively charged buffer ions adsorb at pH 7.0, their respective electrostatic binding to the SAM is clearly detectable during the immobilization phase at pH 6.0, as indicated by the increase of the symmetric  $\nu_s(\text{P}=\text{O})$  at about  $1240$   $\text{cm}^{-1}$ . The observed buffer ion immobilization is further enhanced in the following buffer exchange, which is performed to establish equal conditions in the two systems after the immobilization period. The result is a strongly competitive adsorption between hydrogenase and buffer, which leads to partial desorption in the enzyme immobilized at pH 6.0 (Figure 4), while the amount of protein immobilized at pH 7.0 stays nearly unchanged. This behavior reflects the ionic strength sensitivity of the adsorption process, as observed for other charged proteins.<sup>19</sup>

In contrast to pH 7.0, the subsequent buffer exchange does not lead to any detectable changes in the amide I/amide II ratio for the hydrogenase immobilized at pH 6.0. During the immobilization period, the ratio is larger at pH 7.0, but after the buffer exchange, it drops to similar values as observed for pH 6.0 (see Figure S5 of the Supporting Information). This observation suggests a reorientation of the enzyme at pH 6.0 relative to the surface that might be tentatively ascribed to the structural reorganization predicted by MD simulations at pH 6.0 (sim50, *vide infra*).

Another important insight from the SEIRA measurements is the relative intensity of the CO bands, which can be taken as a measure of the distance  $d$  of the active site of the protein to the Au surface, as the surface enhancement decreases with  $1/d^6$  (Figure 6).<sup>42</sup> The clear difference between the respective intensities for hydrogenase immobilized at pH 6.0 and 7.0 indicates that the relative distance between the gold surface and active site is pH-dependent, suggesting that the distance is larger after immobilization at pH 7.0.

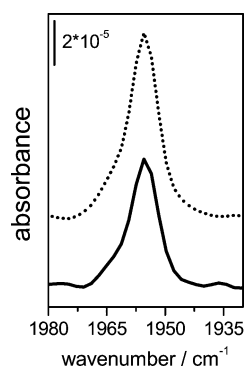


**Figure 6.** Comparison of the CO absorption band of the immobilized (DvMF [NiFe]) hydrogenase recorded with SEIRA spectroscopy after 45 min at pH 6 (···) and pH 7 (—).

The subsequent addition of KCl leads to enzyme desorption, proving the predominantly electrostatic type of interactions between the hydrogenase and the SAM (Figure 4). In fact, the stepwise increasing KCl concentration results in a decreasing amount of immobilized protein in both systems. Furthermore, stronger changes in the amide I/amide II ratio are visible in both systems, which may reflect changes in the orientation of the hydrogenase relative to the surface induced by the high ionic strength or partial desorption (see Figure S5 of the Supporting Information).

**MD Simulations. Interacting Residues.** The initial adsorption of the [NiFe] hydrogenase on the SAM is analyzed by three descriptors: the minimal separation distance between selected amino acids of the [NiFe] hydrogenase and the SAM,

the number of contacts between the enzyme and the SAM, and the interaction energy between the two interaction partners. Because these theoretical calculations are restricted to the nanosecond time scale, they only provide information of the first contacts that can be established between the two interaction partners.

For the sake of consistency and in line with previously employed procedures,<sup>18,19</sup> we denote those protein residues in a minimal separation distance of 5 Å to the SAM as “adsorbed” and define the number of contacts as all protein atoms in a range of 5 Å from the SAM.

Analysis of the MD simulations indicates that, in all simulations, the negatively charged patch of the small subunit facing the surface is attracted by the SAM. Because of the favorable electrostatics, the first adsorption step occurred within ca. 2 ns. Evaluation of the minimal SAM distance of selected amino acids and the number of contacts (Figure 7) clearly reveals the importance of the glutamic acid cluster and the carboxylated C-terminal Ala-264 for adsorption (Figure 8). The glutamic acids, namely, Glu-195, Glu-198, Glu-207, and Glu-216, are located adjacent to the distal [FeS] cluster and might be important for electron transfer.<sup>9,43</sup> Their adsorption is a key event for immobilization. Particularly in the simulations with a high degree of protonation (sim33 and sim50), they act as an anchor for other residues, which adsorb subsequently.

Additionally, the number-of-contacts analysis explicitly reveals the dependence of the adsorption strength on the degree of SAM ionization, which reaches a maximum at a certain point and does not increase any further beyond this level. For example, the number of contacts in sim33 reaches its

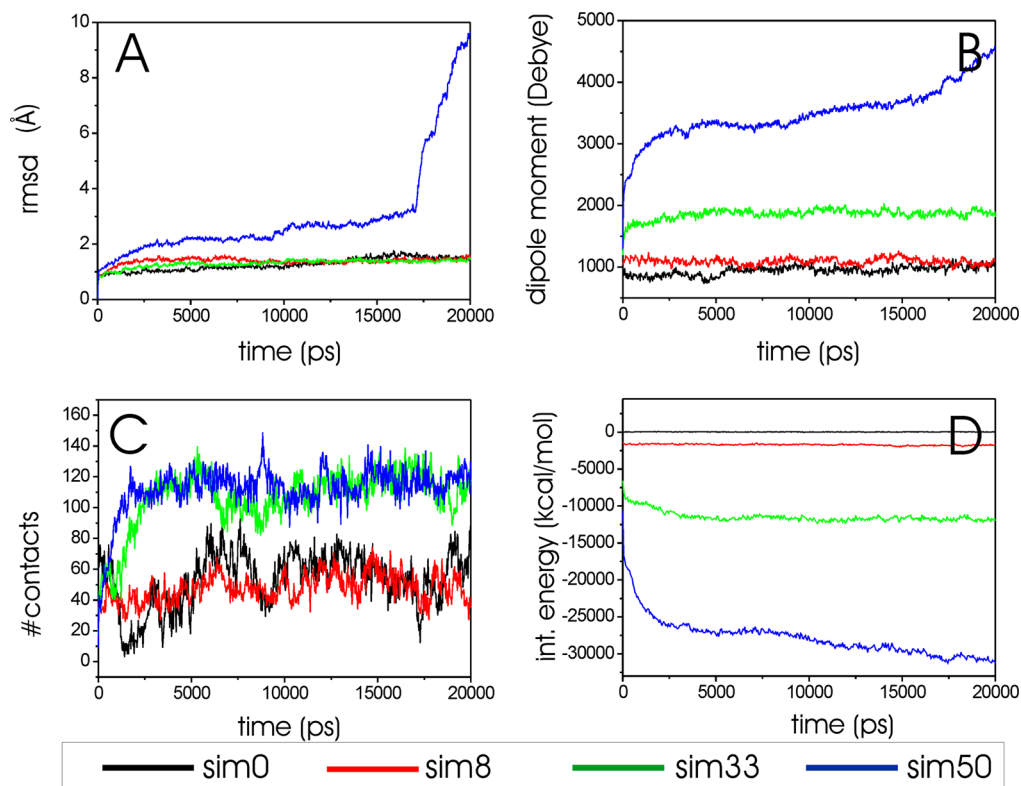


**Figure 7.** Evolution of the rmsd of the (A) hydrogenase backbone, (B) dipole moment of the enzyme, (C) number of contacts between the protein and the SAM, and (D) interaction energy between the hydrogenase and the surface, over time. The different model systems, sim0, sim8, sim33, and sim50, are colored in black, red, green, and blue, respectively.

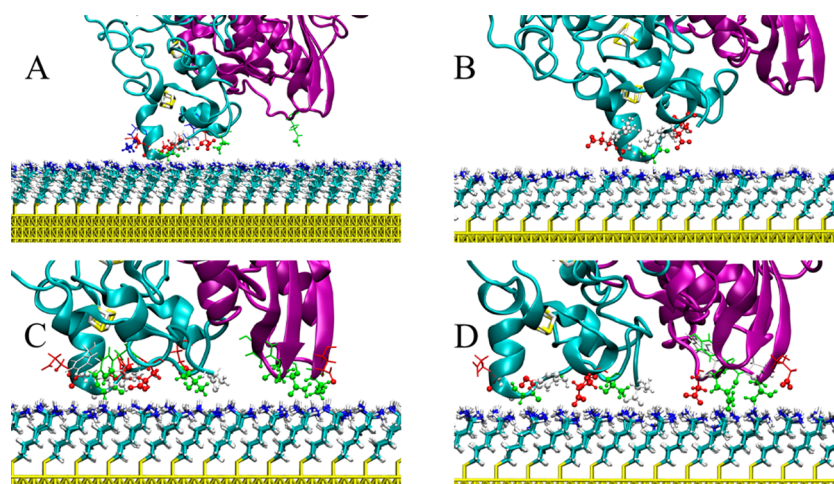


**Figure 8.** Enzyme–SAM interface after 20 ns MD simulation for models (A) sim0, (B) sim8, (C) sim33, and (D) sim50. The protein backbones of the large and small subunits are colored in violet and cyan, respectively. Protein side chains within 5 Å of the SAM are denoted as spheres, and their corresponding bonds are indicated by the stick representation according to their type.

maximum of around 115 contacts after ca. 2.5 ns and then fluctuates around this value.

The systems without (sim0) and with (sim8) low SAM ionization shows initially a weak adsorption of the small subunit with  $58 \pm 12$  and  $51 \pm 9$  contacts on average, respectively. Furthermore, the two models with a higher protonation level exhibit an increase in the number of contacts to  $87 \pm 8$  and  $74 \pm 6$  for the 33 and 50% protonated SAMs, respectively (Table 1). It is remarkable that the number of contacts under low

**Table 1.** Average Values of the Number of Contacts between the Hydrogenase and the SAM, the Small Subunit and the SAM, and the Large Subunit and the SAM<sup>a</sup>

	number of contacts		
	hydrogenase–SAM	small subunit–SAM	large subunit–SAM
sim0	$59 \pm 13$	$58 \pm 12$	$1 \pm 1$
sim8	$51 \pm 9$	$51 \pm 9$	$0 \pm 1$
sim33	$115 \pm 10$	$87 \pm 8$	$29 \pm 5$
sim50	$115 \pm 9$	$74 \pm 6$	$41 \pm 6$

<sup>a</sup>The average values are obtained from the last 10 ns of the MD simulations.

(sim0 and sim8) and high (sim33 and sim50) ionization levels differs considerably, but within the two clusters (sim0–sim8 and sim33–sim50), it is nearly equal and the values lie within the error bars.

Additionally, it is noticeable that the mainly electrostatic driven adsorption dynamics of the large subunit is strongly dependent upon the charge density of the SAM, which is reflected in positive correlation between the number of contacts

and the level of ionization (Table 1). While under low levels of SAM protonation, the large subunit interacts only sporadically with the surface; it is immobilized in conjunction with the small subunit on a highly charged SAM. The most important residues in this adsorption process under a high degree of ionization are Glu-452 and Asp-446 (see Figure 8), while the adsorption of the latter is delayed by ca. 1 ns in sim33.

In general, it is clearly visible that the total number of contacts strongly depends upon the ionization level of the SAM. A higher surface charge leads to an increasing number of contacts (Table 1). This observation is an outcome of two facts. At first, the hydrogenase is pulled closer to the SAM with an increasing surface charge (Table 2), and second, the large subunit is only, at least on this time scale, adsorbing on the surface under high electric field conditions, triggered by a high SAM ionization level. Additionally, the strong adsorption of the large subunit leads to a tilting of the [NiFe] hydrogenase and a slight weakening of the interaction between the small subunit and the monolayer. This conclusion can be drawn by comparing the adsorption interfaces of sim33 and sim50 shown in Figure 8. While the very strong interaction between the small subunit and the SAM in sim33 is weakened in sim50, the loose contact of the large subunit with the surface in sim33 is tightened further in sim50 (Table 1). Possibly, this reduced interaction between the small subunit and SAM in sim50 might affect the electron transfer between the [NiFe] hydrogenase and the surface as a result of a slightly increased separation distance between the distal FeS cluster and the monolayer.

**Protein Stability.** Previous studies dealing with the adsorption of cytochrome *c* on carboxyl-terminated SAMs showed, on the one hand, a positive correlation between the

**Table 2.** Average Values of the Interaction Force between Hydrogenase and SAM, the Interaction Energy between Hydrogenase and SAM, and the Distance between the Ni Atom of the Active Site and the Gold Surface<sup>a</sup>

	interaction force (hydrogenase–SAM) ( $\text{kcal mol}^{-1} \text{Å}^{-1}$ )	interaction energy (hydrogenase–SAM) ( $\text{kcal mol}^{-1}$ )	distance (Au–Ni) (Å)
sim0	$-13 \pm 6$	$19 \pm 17$	$51 \pm 0.8$
sim8	$-71 \pm 7$	$-1777 \pm 83$	$49.3 \pm 1.2$
sim33	$-324 \pm 17$	$-11840 \pm 246$	$44.4 \pm 0.5$
sim50	$-599 \pm 23$	$-29775 \pm 877$	$44.5 \pm 0.3$

<sup>a</sup>The average values are obtained from the last 10 ns of the simulations.

adsorption strength and the level of ionization of the monolayer but, on the other hand, stronger conformational changes of the protein with an increasing charge density of the SAM.<sup>21</sup> This effect has to be considered carefully to obtain strongly bound but intact and catalytically active enzyme molecules on the surface. Therefore, one has to find a trade-off between the adsorption strength and protein stability by changing the pH of the system. To analyze protein stability, we take into account the radius of gyration, the rmsd, and the evolution of the dipole moment.

**Radius of Gyration.** The radius of gyration is a measure for the size and shape of a protein. Changes in the radius of gyration indicate variations in the protein conformation. Our simulations demonstrate a slight increase of the radius of gyration of the [NiFe] hydrogenase in the initial phase of all simulations, which is also observed when the hydrogenase is exposed to solvent only (see Figure S6 of the Supporting Information). Contacts of the enzyme with the solvent molecules and the surface induce a small increase of the radius of gyration from initially 24.8 to ca. 25.3 Å (see Figure S6 of the Supporting Information). These conformational changes appear within ca. 100 ps and are a result of the interplay of mostly hydrophilic amino acids and the solvent. Afterward, the radius of gyration remains stable in all systems, except for sim50, where we observed a steady increase during the simulation until it jumps abruptly to values greater than 27 Å after approximately 17 ns. This evolution reflects structural rearrangements within the [NiFe] hydrogenase in sim50, starting with small but steady changes and eventually resulting in a significant reorganization, particularly in the remote region of the large subunit (130–165) (see the rmsf section).

In all other systems, the changes in the radius of gyration are very similar to the behavior of the enzyme in solution without any adsorption-induced effects.

**Dipole Moment.** Analysis of the dipole moment of the [NiFe] hydrogenase indicates a strong effect of the surface ionization on the protein side chains. During the first step of the adsorption (0–100 ps), the dipole moment of the hydrogenase increases as a function of the charge density of the SAM. While protonation levels of 0 and 8% lead to no or only to a slight increase of the dipole moment to ~1100 D, respectively, the dipole moment of the hydrogenase in sim50 goes up to more than 2500 D (Figure 7B). The prompt change in the dipole moment strength in the beginning of the simulation, similar to the effect described for the radius of gyration, results from reorientations of the protein side chains located at the protein surface, indicating very high flexibility. From the interaction with the electric field induced by the SAM, these chains are attracted or repelled by the surface according to their electrostatic properties. During the MD of sim50, a further increase in the dipole moment of the hydrogenase to more than 3000 D indicates additional structural rearrangements besides the initial reorientation of the protein side chains and is mainly related to the interaction of the large subunit with the SAM. The resulting tilting of the enzyme is partially noticed in sim33 but without a further increase in the dipole moment, which stays relatively stable at ca. 1900 D.

A comparison of the dipole moment of the protein in bulk solution and immobilized on the uncharged SAM (sim0) confirms the hypothesis that a neutrally charged SAM does not perturb the protein structure. Evolution of the dipole moments

in sim0 and in bulk exhibit a very similar behavior (see Figure S7 of the Supporting Information).

**rmsd.** The rmsd is a measure of the structural similarity between two structures. Evaluation of the rmsd of all heavy atoms of the protein during the MD simulations confirms the observed correlation between the surface charge density of the SAM and protein stability (Figure 7A). In all systems, except in sim50, the [NiFe] hydrogenase stays very close to its initial structure and the corresponding rmsd values do not exceed the 2.5 Å borders. The rmsd of the hydrogenase in bulk solution lies below 2 Å. This difference reflects the influence of the surface on the protein and especially on the side chains of the protein. In addition, the analysis of the rmsd of the protein backbone confirms the high stability of secondary structure elements monitoring a fluctuation around 1.5 Å, which indicates a stable protein and is matching the value obtained in bulk solution. These findings clearly show that, except for sim50, only the protein side chains are affected upon immobilization and that the secondary structure remains nearly unchanged, at least during an early adsorption phase.

In contrast to these observations, the hydrogenase in sim50 undergoes a stronger structural reorganization on the highly charged surface. The rmsd increases to more than 3 Å within 5 ns of simulation, where it stays stable for another 5 ns until it increases again and reaches 10 Å after 20 ns. These findings indicate that a high surface charge has a noticeable influence on the protein stability and even secondary structure elements are affected by the strong electric field induced by the highly protonated SAM.

**rmsf.** The rmsf of the C<sub>α</sub> atoms of all amino acids gives information about the flexibility of single residues in the protein. By computing rmsf, one can specifically identify regions of the macromolecule that undergo high structural changes and fluctuations during time. Analysis of the rmsf of the [NiFe] hydrogenase on the SAMs with different protonation levels reveals that only sim50 exhibits prominent fluctuations (see Figure S8 of the Supporting Information). On top of the overall rather strong fluctuations, a region of the large subunit (130–165) shows a prominent rmsf value of more than 20 Å. Surprisingly, this region is not located adjacent to the surface but in a remote position more than 70 Å away from the gold film (see Figure S9 of the Supporting Information). Because of the large number of lysine and arginine residues, namely, Lys-133, Arg-136, Lys-144, Lys-145, Lys-152, Lys-157, and Lys-159, the region exhibits a high positive charge, which accounts for a strong repulsion from the surface. After ca. 17 ns, the region spanned by two helices, which are connected by a loop region, flips away from its initial position into the bulk solution and points away from the surface. During this process, the helical structure is partially conserved but the embedment in the protein is altered.

A comparison of the fractions of residues located in secondary structure elements in the simulations under different pH values monitors very similar results for sim0, sim8, and sim33 ( $\alpha$ -helices, ca. 42–43%;  $\beta$ -sheets, ca. 15%) but slightly decreasing fractions for sim50 ( $\alpha$ -helices, ca. 36%;  $\beta$ -sheets, ca. 12%). This loss of structural elements is another indicator for protein rearrangements at low pH.

**Interaction Energies between the Hydrogenase and Surface.** The strength of adsorption of the hydrogenase onto a SAM can be quantified through the computation of the interaction energies ( $E_{\text{int}}$ ) between the surface and the enzyme. The evolution of the interaction energies during the MD

simulation are plotted for the four model system in Figure 7D. For these calculations, the surface is defined as the SAM together with the 5 Å adlayer of water molecules and ions.

For all models, with the exception of model sim50, the interaction energies remain practically constant, reflecting once again the stability of the protein and its interaction with the SAM. As expected, the strength of the interaction is proportional to the degree of protonation of the SAM: for a neutral SAM,  $E_{\text{int}}$  is almost negligible (on average, only 22 kcal/mol); for sim8, we predict an  $E_{\text{int}}$  of only  $-1700$  kcal/mol, which significantly increases to  $-12\,000$  kcal/mol in sim33; and for sim50,  $E_{\text{int}}$  reaches a value of ca.  $30\,000$  kcal/mol after 20 ns. Furthermore, for the neutral SAM, the positive sign of the interaction energy reflects the repulsive character of the very weak interaction. For all positive-charged SAMs, however, attractive interactions between the surface and protein are predicted.

**Comparison between Experiment and Theory.** The determination of the  $pK_a$  value of the amino-terminated SAM allows for a direct comparison between the immobilization conditions and the results of the SEIRA experiments to the theoretical prediction obtained from the MD simulations.

At pH 7.0, the SEIRA measurements are in good agreement with theory (sim8) and validate the weak but stable adsorption of the hydrogenase. At pH 6.0, however, the interpretation is much more complex but, anyway, consistent among the two techniques. The SEIRA measurements monitor a similar amount of immobilized protein under both low and high pH conditions during the immobilization phase, which is, upon a first glance, in conflict with the MD simulations (sim50), where the number of contacts between the enzyme and SAM is higher under lower pH conditions. Closer analysis suggests that this discrepancy is most likely due to competitive buffer adsorption, which is not taken into account in the MD simulations, where equal ionic strength conditions are used in all systems. The buffer effect is clearly observed in the SEIRA experiment, where at pH 6.0, a partial desorption of the immobilized hydrogenase is observed after replacing the buffer solution, accompanied by binding of phosphate ions. At pH 7.0, this effect is much weaker, resulting in an observed stable immobilization. Another reason for discrepancies between theory and experiment might be that possible changes in the protonation state of individual amino acids, brought about by the transition from the dissolved to the immobilized state, cannot be considered in the simulations.

Furthermore, changes in the hydrogenase orientation with respect to the SAM are observed in the MD simulations as well as in the experiments (*vide supra*). The pH-dependent reorientation of the enzyme is reflected in the simulations by the decreasing distance between the gold and the active site (Table 2), which can be related to the increase of the CO band intensity with a decreasing pH (Figure 6) in the experiments. In addition, the structural reorganization within the enzyme and the related initial reorientation simulated for sim50 (pH 6.0) may be related to the variations in the amide I spectral region compared to the spectra measured at pH 7 (see Figure S10 of the Supporting Information), and the different amide I/amide II ratios monitored at the two pH values indicate different protein orientations relative to the surface (see Figure S5 of the Supporting Information). Despite this good qualitative agreement between the structural changes derived from experiment and simulation, two specific methodological restrictions have to be pointed out to adequately assess the potential and

limitations of the present combined theoretical and experimental analysis. First, the two methods refer to different time scales (minutes versus nanoseconds). Thus, potential slow structural rearrangements of the immobilized protein, leading to the final state of the protein monitored by SEIRA spectroscopy, are not covered by the MD simulations. That means that, with MD simulations, we are only able to investigate a very early stage of the protein adsorption process. Second, SEIRA spectroscopy probes the protein structural changes in close vicinity to the surface such that the major changes predicted in the MD simulations of sim50 are presumably not detectable in the experiment.

## CONCLUSION

The present study has shown that the combination of MD simulations and SEIRA spectroscopy may be used to guide a rational design of biocompatible surface coatings for the immobilization of enzymes under preservation of their native structure. Although the experimental method does not provide information about the three-dimensional structure of the adsorbed protein, it allows for qualitative conclusions about the secondary and tertiary structure changes and protein reorientations. Such conclusions may be related to the protein structural changes predicted by the MD simulations, although only in the first nanosecond time scale. The prerequisite for such correlations is, however, that experiments and simulations are carried out under “similar conditions”. In the present case of a predominantly electrostatic binding of the target enzyme, the crucial parameter is the surface charge density. This quantity has been derived from electrochemical experiments yielding the effective  $pK_a$  of the SAM. Thus, the protonation state of the SAM head groups in the MD simulations can be adjusted according to the pH to which the individual SEIRA measurements are referred. In this way, the present case study on the immobilization of hydrogenase afforded a good qualitative agreement between the MD simulations and spectroscopic experiments such that the present combined experimental and theoretical approach promised to become an important tool for optimizing immobilization conditions for enzymes on solid supports.

## ASSOCIATED CONTENT

### Supporting Information

Figures containing the CV traces for SAM titration, additional SEIRA spectra, evolution of the radius of gyration, rmsf during the MD simulation, and structural alignment of the initial and end conformations of hydrogenase in sim50. This material is available free of charge via the Internet at <http://pubs.acs.org>.

## AUTHOR INFORMATION

### Corresponding Author

\*E-mail: [andrea.mroginski@tu-berlin.de](mailto:andrea.mroginski@tu-berlin.de)

### Notes

The authors declare no competing financial interest.

## ACKNOWLEDGMENTS

This research has been financed by the Deutsche Forschungsgemeinschaft Cluster of Excellence “Unicat”. The authors are grateful to Prof. Wolfgang Lubitz for kindly supplying the DvMF enzyme. The authors thank the “Senat Berlin” for financial support (Nachhaltige Chemie), the “Norddeutscher Verbund für Hoch- und Höchstleistungsrechnen” (HLRN) for

providing computer power, the Alexander-von-Humboldt Foundation (to Diego Millo), and The Netherlands Organisation for Scientific Research (NWO), Grant 722.011.003 (to Diego Millo).

## ABBREVIATIONS USED

SAM, self-assembled monolayer; SEIRA, surface-enhanced infrared absorption; CV, cyclic voltammetry; MD, molecular dynamics; *DvMF*, *Desulfovibrio vulgaris* Miyazaki F; rmsd, root-mean-square deviation; rmsf, root-mean-square fluctuation

## REFERENCES

- (1) Adams, M. W. W.; Mortenson, L. E.; Chen, J. S. Hydrogenase. *Biochim. Biophys. Acta, Rev. Bioenerg.* **1980**, *594*, 105–176.
- (2) Lojou, E. Hydrogenases as catalysts for fuel cells: Strategies for efficient immobilization at electrode interfaces. *Electrochim. Acta* **2011**, *56*, 10385–10397.
- (3) Vignais, P. M.; Billoud, B. Occurrence, classification, and biological function of hydrogenases: An overview. *Chem. Rev.* **2007**, *107*, 4206–4272.
- (4) Vincent, K. A.; Cracknell, J. A.; Lenz, O.; Zebger, I.; Friedrich, B.; Armstrong, F. A. Electrocatalytic hydrogen oxidation by an enzyme at high carbon monoxide or oxygen levels. *Proc. Natl. Acad. Sci. U.S.A.* **2005**, *102*, 16951–16954.
- (5) Vincent, K. A.; Cracknell, J. A.; Clark, J. R.; Ludwig, M.; Lenz, O.; Friedrich, B.; Armstrong, F. A. Electricity from low-level H<sub>2</sub> in still air—An ultimate test for an oxygen tolerant hydrogenase. *Chem. Commun.* **2006**, 5033–5035.
- (6) Lyon, E. J.; Shima, S.; Boecher, R.; Thauer, R. K.; Grevels, F. W.; Bill, E.; Roseboom, W.; Albracht, S. P. J. Carbon monoxide as an intrinsic ligand to iron in the active site of the iron–sulfur-cluster-free hydrogenase H<sub>2</sub>-forming methylenetetrahydromethanopterin dehydrogenase as revealed by infrared spectroscopy. *J. Am. Chem. Soc.* **2004**, *126*, 14239–14248.
- (7) Vignais, P. M.; Billoud, B.; Meyer, J. Classification and phylogeny of hydrogenases. *FEMS Microbiol. Rev.* **2001**, *25*, 455–501.
- (8) Volbeda, A.; Garcin, E.; Piras, C.; De Lacey, A. L.; Fernandez, V. M.; Hatchikian, E. C.; Frey, M.; Fontecilla-Camps, J. C. Structure of the [NiFe] hydrogenase active site: Evidence for biologically uncommon Fe ligands. *J. Am. Chem. Soc.* **1996**, *118*, 12989–12996.
- (9) Fontecilla-Camps, J. C.; Volbeda, A.; Cavazza, C.; Nicolet, Y. Structure/function relationships of [NiFe]- and [FeFe]-hydrogenases. *Chem. Rev.* **2007**, *107*, 4273–4303.
- (10) Pierik, A. J.; Roseboom, W.; Happe, R. P.; Bagley, K. A.; Albracht, S. P. J. Carbon monoxide and cyanide as intrinsic ligands to iron in the active site of [NiFe]-hydrogenases. *J. Biol. Chem.* **1999**, *274*, 3331–3337.
- (11) Stein, M.; Lubitz, W. Quantum chemical calculations of [NiFe] hydrogenase. *Curr. Opin. Chem. Biol.* **2002**, *6*, 243–249.
- (12) De Lacey, A. L.; Fernandez, V. M.; Rousset, M.; Cammack, R. Activation and inactivation of hydrogenase function and the catalytic cycle: Spectroelectrochemical studies. *Chem. Rev.* **2007**, *107*, 4304–4330.
- (13) Ogata, H.; Lubitz, W.; Higuchi, Y. [NiFe] hydrogenases: Structural and spectroscopic studies of the reaction mechanism. *Dalton Trans.* **2009**, 7577–7587.
- (14) Cracknell, J. A.; Vincent, K. A.; Armstrong, F. A. Enzymes as working or inspirational electrocatalysts for fuel cells and electrolysis. *Chem. Rev.* **2008**, *108*, 2439–2461.
- (15) Millo, D.; Pandelia, M. E.; Utesch, T.; Wisitruangsakul, N.; Mroginski, M. A.; Lubitz, W.; Hildebrandt, P.; Zebger, I. Spectroelectrochemical study of the [NiFe] hydrogenase from *Desulfovibrio vulgaris* Miyazaki F in solution and immobilized on biocompatible gold surfaces. *J. Phys. Chem. B* **2009**, *113*, 15344–15351.
- (16) Rüdiger, O.; Abad, J. M.; Hatchikian, E. C.; Fernandez, V. M.; De Lacey, A. L. Oriented immobilization of *Desulfovibrio gigas* hydrogenase onto carbon electrodes by covalent bonds for non-mediated oxidation of H<sub>2</sub>. *J. Am. Chem. Soc.* **2005**, *127*, 16008–16009.
- (17) Raut, V. P.; Agashe, M. A.; Stuart, S. J.; Latour, R. A. Molecular dynamics simulations of peptide–surface interactions. *Langmuir* **2005**, *21*, 1629–1639.
- (18) Utesch, T.; Daminelli, G.; Mroginski, M. A. Molecular dynamics simulations of the adsorption of bone morphogenetic protein-2 on surfaces with medical relevance. *Langmuir* **2011**, *27*, 13144–13153.
- (19) Utesch, T.; Sezer, M.; Weidinger, I. M.; Mroginski, M. A. Adsorption of sulfite oxidase on self-assembled monolayers from molecular dynamics simulations. *Langmuir* **2012**, *28*, 5761–5769.
- (20) Wang, Q.; Zhao, C.; Zhao, J.; Wang, J.; Yang, J. C.; Yu, X.; Zheng, J. Comparative molecular dynamics study of  $\alpha\beta$  adsorption on the self-assembled monolayers. *Langmuir* **2009**, *26*, 3308–3316.
- (21) Zhou, J.; Zheng, J.; Jiang, S. Molecular simulation studies of the orientation and conformation of cytochrome *c* adsorbed on self-assembled monolayers. *J. Phys. Chem. B* **2004**, *108*, 17418–17424.
- (22) Wei, T.; Carignano, M. A.; Szleifer, I. Lysozyme adsorption on polyethylene surfaces: Why are long simulations needed? *Langmuir* **2011**, *27*, 12074–12081.
- (23) Zuo, G.; Zhou, X.; Huang, Q.; Fang, H.; Zhou, R. Adsorption of villin headpiece onto graphene, carbon nanotube, and C60: Effect of contacting surface curvatures on binding affinity. *J. Phys. Chem. C* **2011**, *115*, 23323–23328.
- (24) Degefa, T. H.; Schön, P.; Bongard, D.; Walder, L. Elucidation of the electron transfer mechanism of marker ions at SAMs with charged head groups. *J. Electroanal. Chem.* **2004**, *574*, 49–62.
- (25) Rippers, Y.; Utesch, T.; Hildebrandt, P.; Zebger, I.; Mroginski, M. A. Insights into the structure of the active site of the O<sub>2</sub>-tolerant membrane bound [NiFe] hydrogenase of *R. eutropha* H16 by molecular modelling. *Phys. Chem. Chem. Phys.* **2011**, *13*, 16146–16149.
- (26) Brooks, B. R.; Bruccoleri, R. E.; Olafson, B. D.; States, D. J.; Swaminathan, S.; Karplus, M. CHARMM: A program for macromolecular energy, minimization, and dynamics calculations. *J. Comput. Chem.* **1983**, *4*, 187–217.
- (27) Olsson, M. H. M.; Sondergaard, C. R.; Rostkowski, M.; Jensen, J. H. PROPKA3: Consistent treatment of internal and surface residues in empirical pK<sub>a</sub> predictions. *J. Chem. Theory Comput.* **2011**, *7*, 525–537.
- (28) Li, H.; Robertson, A. D.; Jensen, J. H. Very fast empirical prediction and rationalization of protein pK<sub>a</sub> values. *Proteins* **2005**, *61*, 704–721.
- (29) Teixeira, V. H.; Baptista, A. M.; Soares, C. M. Pathways of H<sub>2</sub> toward the active site of [NiFe]-hydrogenase. *Biophys. J.* **2006**, *91*, 2035–2045.
- (30) Rappe, A. K.; Casewit, C. J.; Colwell, K. S.; Goddard, W. A.; Skiff, W. M. UFF, a full periodic table force field for molecular mechanics and molecular dynamics simulations. *J. Am. Chem. Soc.* **1992**, *114*, 10024–10035.
- (31) Widrig, C. A.; Alves, C. A.; Porter, M. D. Scanning tunneling microscopy of ethanethiolate and *N*-octadecanethiolate monolayers spontaneously adsorbed at gold surfaces. *J. Am. Chem. Soc.* **1991**, *113*, 2805–2810.
- (32) Bizzarri, A. R.; Costantini, G.; Cannistraro, S. MD simulation of a plastocyanin mutant adsorbed onto a gold surface. *Biophys. Chem.* **2003**, *106*, 111–123.
- (33) Feller, S. E.; Gawrisch, K.; MacKerell, A. D. Polyunsaturated fatty acids in lipid bilayers: Intrinsic and environmental contributions to their unique physical properties. *J. Am. Chem. Soc.* **2001**, *124*, 318–326.
- (34) Phillips, J. C.; Braun, R.; Wang, W.; Gumbart, J.; Tajkhorshid, E.; Villa, E.; Chipot, C.; Skeel, R. D.; Kale, L.; Schulten, K. Scalable molecular dynamics with NAMD. *J. Comput. Chem.* **2005**, *26*, 1781–1802.
- (35) MacKerell, A. D., Jr.; Bashford, D.; Bellott, M.; Dunbrack, R. L., Jr.; Evanseck, J. D.; Field, M. J.; Fischer, S.; Gao, J.; Guo, H.; Ha, S.; Joseph-McCarthy, D.; Kuchnir, L.; Kuczera, K.; Lau, F. T. K.; Mattos, C.; Michnick, S.; Ngo, T.; Nguyen, D. T.; Prodhom, B.; Reiher, W. E.,

III; Roux, B.; Schlenkrich, M.; Smith, J. C.; Stote, R.; Straub, J.; Watanabe, M.; Wiorkiewicz-Kuczera, J.; Yin, D.; Karplus, M. All-atom empirical potential for molecular modeling and dynamics studies of proteins. *J. Phys. Chem. B* **1998**, *102*, 3586–3616.

(36) Jorgensen, W. L.; Chandrasekhar, J.; Madura, J. D.; Impey, R. W.; Klein, M. L. Comparison of simple potential functions for simulating liquid water. *J. Chem. Phys.* **1983**, *79*, 926–935.

(37) Humphrey, W.; Dalke, A.; Schulten, K. VMD: Visual molecular dynamics. *J. Mol. Graphics* **1996**, *14*, 33–38.

(38) van Gunsteren, W. F.; Berendsen, H. J. C. Algorithms for macromolecular dynamics and constraint dynamics. *Mol. Phys.* **1977**, *34*, 1311–1327.

(39) Darden, T.; York, D.; Pedersen, L. Particle mesh Ewald: An  $N \cdot \log(N)$  method for Ewald sums in large systems. *J. Chem. Phys.* **1993**, *98*, 10089–10092.

(40) Kastenholz, M. A.; Hünenberger, P. H. Influence of artificial periodicity and ionic strength in molecular dynamics simulations of charged biomolecules employing lattice-sum methods. *J. Phys. Chem. B* **2003**, *108*, 774–788.

(41) Soliman, W.; Bhattacharjee, S.; Kaur, K. Adsorption of an antimicrobial peptide on self-assembled monolayers by molecular dynamics simulation. *J. Phys. Chem. B* **2010**, *114*, 11292–11302.

(42) Osawa, M. Surface-enhanced infrared absorption. *Top. Appl. Phys.* **2001**, *81*, 163–187.

(43) Marr, A. C.; Spencer, D. J. E.; Schröder, M. Structural mimics for the active site of [NiFe] hydrogenase. *Coord. Chem. Rev.* **2001**, *219–221*, 1055–1074.